Available online at www.sciencedirect.com

ScienceDirect

journal homepage: http://www.elsevier.com/locate/rpor

Original research article

A surface energy spectral study on the bone heterogeneity and beam obliquity using the flattened and unflattened photon beams

James C.L. Chow[a,b,*], Amir M. Owrangi[a,c]

[a] Department of Radiation Oncology, University of Toronto, Toronto, ON M5G 2M9, Canada
[b] Radiation Medicine Program, Princess Margaret Caner Center, University Health Network, Toronto, ON M5G 2M9, Canada
[c] Department of Medical Physics, Sunnybrook Health Sciences Center, Toronto ON M4N 3M5, Canada

ARTICLE INFO

Article history:
Received 6 May 2015
Received in revised form
30 September 2015
Accepted 5 November 2015
Available online 30 November 2015

Keywords:
Unflattened photon beam
Energy fluence spectrum
Surface dosimetry
Bone heterogeneity
Beam obliquity
Monte Carlo simulation

ABSTRACT

Aim: Using flattened and unflattened photon beams, this study investigated the spectral variations of surface photon energy and energy fluence in the bone heterogeneity and beam obliquity.

Background: Surface dose enhancement is a dosimetric concern when using unflattened photon beam in radiotherapy. It is because the unflattened photon beam contains more low-energy photons which are removed by the flattening filter of the flattened photon beam.

Materials and methods: We used a water and bone heterogeneity phantom to study the distributions of energy, energy fluence and mean energy of the 6 MV flattened and unflattened photon beams (field size = 10 cm × 10 cm) produced by a Varian TrueBEAM linear accelerator. These elements were calculated at the phantom surfaces using Monte Carlo simulations. The photon energy and energy fluence calculations were repeated with the beam angle turned from 0° to 15°, 30° and 45° in the water and bone phantom.

Results: Spectral results at the phantom surfaces showed that the unflattened photon beams contained more photons concentrated mainly in the low-energy range (0–2 MeV) than the flattened beams associated with a flattening filter. With a bone layer of 1 cm under the phantom surface and within the build-up region of the 6 MV photon beam, it is found that both the flattened and unflattened beams had slightly less photons in the energy range <0.4 MeV compared to the water phantom. This shows that the presence of the bone decreased the low-energy photon backscatters to the phantom surface. When both the flattened and unflattened photon beams were rotated from 0° to 45°, the number of photon and mean photon energy increased. This indicates that both photon beams became more hardened or penetrate when the beam angle increased. In the presence of bone, the mean energies of both photon beams increased. This is due to the absorption of low-energy photons by the bone, resulting in more beam hardening.

* *Corresponding author at*: Department of Radiation Physics, Princess Margaret Cancer Center, 610 University Ave., Toronto, ON M5G 2M9, Canada. Tel.: +1 416 946 4501; fax: +1 416 946 6566.
E-mail address: james.chow@rmp.uhn.on.ca (J.C.L. Chow).

http://dx.doi.org/10.1016/j.rpor.2015.11.001

Conclusions: This study explores the spectral relationships of surface photon energy and energy fluence with bone heterogeneity and beam obliquity for the flattened and unflattened photon beams. The photon spectral information is important in studies on the patient's surface dose enhancement using unflattened photon beams in radiotherapy.

1. Background

To make the delivery of some recent radiotherapy techniques such as intensity modulated radiotherapy and volumetric modulated arc therapy more efficient, medical linear accelerator capable of producing unflattened photon beams was developed.[1–5] With the removal of the flattening filter which generates a uniform beam profile for 3D-conformal radiotherapy, the output of the photon beam is highly increased.[6,7] For example, the Varian TrueBEAM linear accelerator can produce 1400 monitor units (MU) and 2400 MU per minute for the 6 and 10 MV photon beams, respectively. This dose rate from the flattening-filter free linear accelerator is about 2–3 times higher than the conventional accelerator producing flattened photon beams, and can shorten the treatment time.[8,9] Therefore, the patient throughput can be increased. Moreover, for the increasingly popular hypofractionated and stereotactic body radiotherapy, the unflattened photon beam is useful.[10–15] As some patients may be undergoing some kind of breath hold technique to manage respiratory motion issues, a fast treatment is necessary to take into account the patient's comfort and intrafraction organ motion.[12]

While it is advantageous to use an unflattened photon beam in radiation dose delivery, the exclusion of the flattening filter from the beam has some dosimetric concerns. The removal of the flattening filter largely decreases the beam attenuation and increases the photon fluence, but it also affects the photon energy distribution or beam quality.[16–18] The presence of the flattening filter uses to remove a large number of low-energy photons and results in beam hardening. For the unflattened photon beam, however, these low-energy photons are part of the beam and contribute to the dose deposition in the photon beam build-up region close to the patient surface. Compared to the flattened photon beam, though unflattened beam has less head scatter and leakage, measurements and Monte Carlo simulations have found that irradiation of the unflattened photon beam results in a higher surface dose than the flattened beam.[19,20] This indicates that the low-energy photons may play an important role in the surface dose enhancement of the unflattened beam. It is therefore worthwhile to compare the photon energy and energy fluence spectra between the flattened and unflattened beams. For unflattened beams, it is useful to identify in which low-energy range the photons have a higher intensity.

Apart from the presence of extra low-energy photons in the unflattened photon beams, it is well-known that the surface dose is also affected by heterogeneities close to the build-up region and the variation of beam obliquity.[21,22] Heterogeneities close to the patient surface such as bone, affects the backscatter contribution to the surface dose. This dosimetric impact is an issue in the lung and head-and-neck radiotherapy,[23] where the rib and skull are close to the patient surface and the bone backscatter would affect the photon beam energy spectrum. It is therefore worthwhile to investigate the different effects of the flattened and unflattened photon beams on the backscatter photons arising from the bone heterogeneity due to their different beam qualities. Furthermore, as the patient's external contour is curved and not perfectly perpendicular to the incident photon beam, beam obliquity is inevitable and would affect the surface dose in radiotherapy. It is found from measurements and Monte Carlo simulations that surface dose increases with an increase of beam angle.[21,24] However, spectral variations of photon energy and energy fluence in the beam obliquity for the flattened and unflattened beams have still not been reported.

2. Aim

In most previous dosimetric studies on unflattened photon beams, the flattening filter from a conventional linear accelerator was not designed in dose measurements or Monte Carlo simulations, respectively.[7,18,25–27] It should be noted that these conventional linear accelerators were not designed to produce clinical unflattened photon beams. In this study, the Varian TrueBEAM linear accelerator specifically designed to produce clinical unflattened photon beams was used. Photon energy and energy fluence spectra at surface were calculated by Monte Carlo simulations using the water and bone heterogeneous phantom (bone phantom). Through spectral comparisons of photon energy and energy fluence, variations of the unflattened beam quality in the presences of bone heterogeneity and beam obliquity were analyzed.

3. Materials and methods

3.1. *Water and bone heterogeneous phantom*

To compare the photon energy and energy fluence spectra with and without the bone heterogeneity, a water and bone phantom with the same dimension (13 cm × 20 cm × 20 cm) was used in our Monte Carlo simulations. The bone phantom in Fig. 1 has a bone layer with thickness equal to 2 cm. This bone layer was sandwiched by two water layers with thicknesses equal to 1 cm (on top of the bone layer) and 10 cm (under the bone layer). The bone layer was positioned within the build-up region of the 6 MV photon beam with the depth of maximum dose equal to 1.5 cm. In the Monte Carlo simulation, the ICRPBONE700ICRU bone in the EGSnrc-based Pegs4 dataset was used (ICRP 1975).[28] The density of the bone layer

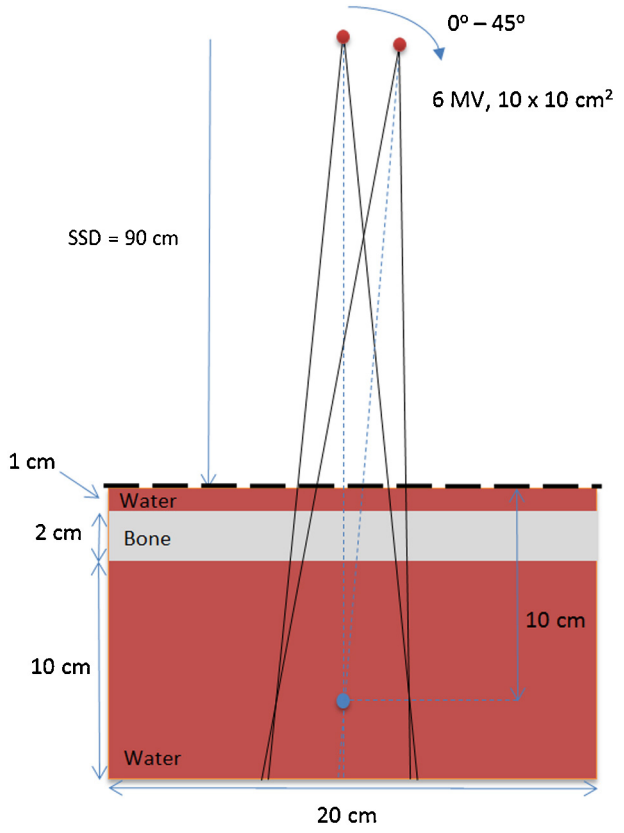

Fig. 1 – Schematic diagram (not to scale) showing the calculation geometry of the bone phantom irradiated by the 6 MV flattened and unflattened photon beams (field size = 10 cm × 10 cm). The isocenter was at 10 cm depth from the phantom surface. The photon beams were rotated from 0° to 45° and the thickness of bone was equal to 2 cm. Photon energy and energy fluence spectra were calculated at the phantom surface (horizontal broken line). Calculations using the same beam geometry but a water phantom with the bone replaced by water were repeated for comparison.

was equal to 1.75 g/cm^3, and the bone contained H, C, N, O, Mg, P, S, Ca and Zn with weight ratios equal to 4.69, 1.2, 0.29, 2.79, 0.0091, 0.34, 0.098, 0.52 and 0.00015, respectively.

3.2. *Beam calculation geometries*

6 MV flattened and unflattened photon beams with field size equal to 10 cm × 10 cm produced by the Varian TrueBEAM linear accelerator were used. The water and bone phantom were irradiated by the photon beams with isocenter located at 10 cm depth of the phantom (Fig. 1). The source-to-surface distance was equal to 90 cm. Apart from calculating the photon energy and energy fluence spectra for the flattened and unflattened beams with beam angle set to zero at the phantom surface (i.e. horizontal broken line in Fig. 1), spectral calculations were repeated with photon beams rotated to 15°, 30° and 45° clockwise for the water and bone phantom.

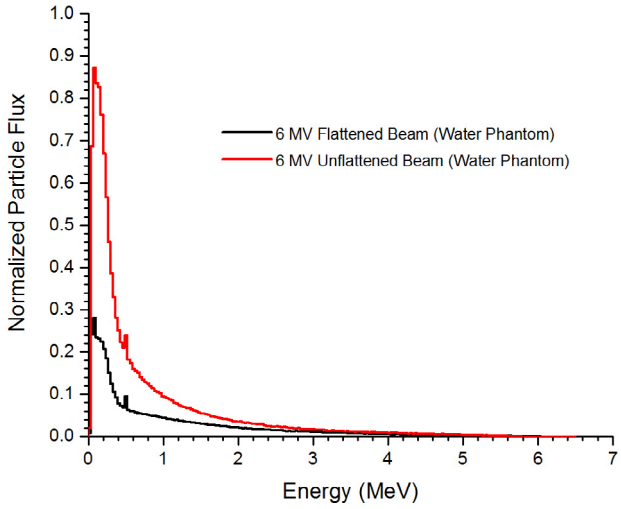

Fig. 2 – Photon energy spectra at the water phantom surface for the 6 MV flattened and unflattened photon beams.

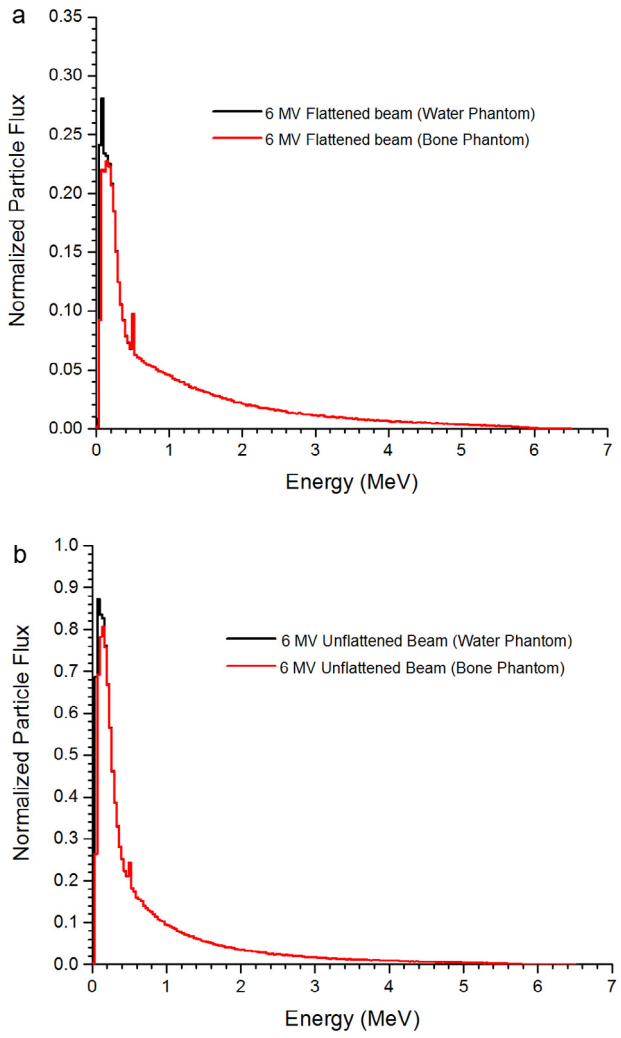

Fig. 3 – Photon energy spectra at the water and bone phantom surface for the 6 MV (a) flattened and (b) unflattened photon beams.

3.3. *Monte Carlo simulations*

3.3.1. *Phase-space files of the flattened and unflattened photon beams*

The Geant4 and EGSnrc-based Monte Carlo code were used to model the Varian TrueBEAM linear accelerator.[29,30] The gantry head of the linear accelerator was modelled by the Varian Monte Carlo study team using the Geant4 code.[31–33] Phase-space files containing information of the particle's type, location, orientation and energy for the 6 MV flattened and unflattened photon beams were then generated by the team and used in our simulations.[34] Since the scoring planes (planes at which the simulated beam phase-space data are scored) of the phase-space files generated by the Geant4 code were merely up to the position above the jaws, the BEAMnrc code[35] was used to transport the Geant4 phase-space file through the secondary collimator (X–Y jaws). The reason to use the BEAMnrc code is that complex simulation programming related to the geometry of jaws can be avoided by taking advantage of the component-module approach of the code, which is not found in the Geant4. The phase-space files generated by the BEAMnrc contained particle data of the 6 MV flattened and unflattened photon beams with field size equal to 10 cm × 10 cm at the isocenter. In the verification of the Monte Carlo simulations, each phase-space file (contained 1×10^9 particles) from the EGSnrc was verified by comparing the Monte Carlo dosimetry with the commissioning data acquired from measurements using ionization chamber and scanning water tank. By comparing the percentage depth doses calculated and measured by Monte Carlo simulation and ionization chamber as shown elsewhere,[20,36] it is found that such dosimetric deviation was within 1% and therefore the phase-space files of the flattened and unflattened photon beams were verified.

3.3.2. *Calculations of the photon energy and energy fluence spectra*

Photon energy and energy fluence spectra were calculated from phase-space files (Section 3.3.1) including the water and bone phantom in the Monte Carlo model using the BEAMnrc. The scoring plane of the phase-space file with multiple crossers (backscattered photons) was set at the phantom surface as shown in the horizontal broken line in Fig. 1. The

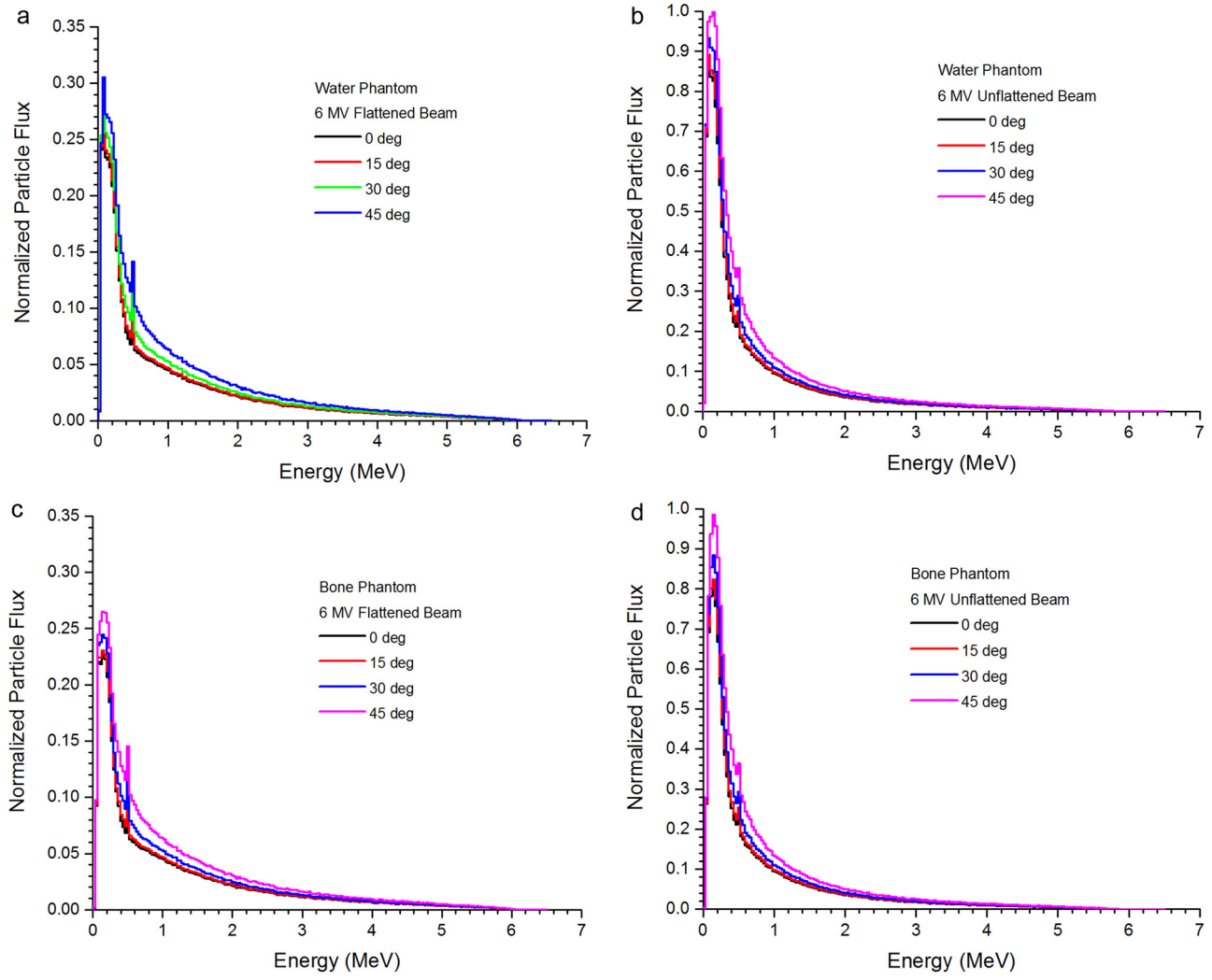

Fig. 4 – The variations of photon energy spectra in beam angle for the 6 MV (a) flattened photon beams (water phantom), (b) unflattened photon beams (water phantom), (c) flattened photon beams (bone phantom) and (d) unflattened photon beams (bone phantom).

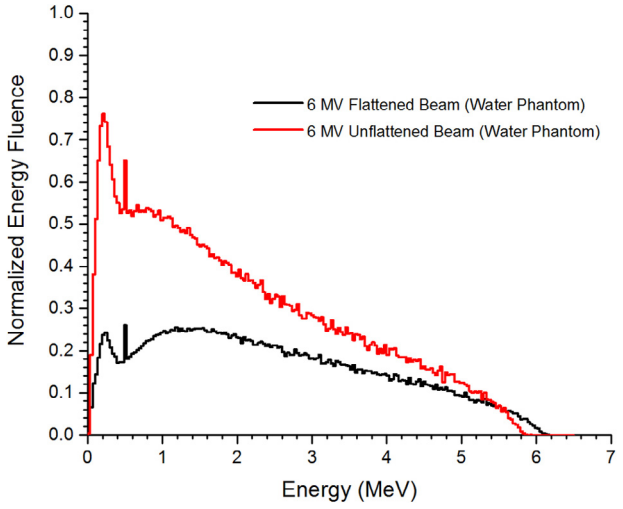

Fig. 5 – Photon energy fluence spectra at the water phantom surface for the 6 MV flattened and unflattened photon beams.

EGSnrc-based BEAMDP code[35] was used to determine the photon energy and energy fluence spectra based on the phase-space data. The number of bins in each spectrum was set to 650 with energy range from 0 to 6.5 MeV. To compare the flattened and unflattened photon beams regarding beam obliquity, Monte Carlo simulations were repeated in both the water and bone phantom with beam angles equal to 15°, 30° and 45°.

4. Results

The photon energy spectra of the 6 MV flattened and unflattened photon beams at the water phantom surface are shown in Fig. 2. In this study, the particle fluence is defined as the quotient *dN* by *dA*, where *dN* is the number of photons entering an imaginary sphere with cross-sectional area equal to A. Similarly, energy fluence is the quotient of *dE* by *dA*, where *dE* is the total energy of all photons entering the sphere. For bone heterogeneity, the photon energy spectra of the flattened and unflattened beams in the water and bone phantom are shown in Fig. 3(a) and (b). For beam obliquity, Fig. 4(a) and (b) shows the photon energy spectra of the flattened and unflattened beams with beam angles equal to 0°, 15°, 30° and 45° at the water phantom surface, while Fig. 4(c) and (d) shows the corresponding spectra at the bone phantom surface. All photon energy spectra (Figs. 2–4) were calculated using the same flattened and unflattened beam phase-space files with the same number of particles, and normalized to the maximum intensity in all beam calculation geometries (different beam angles and phantoms) for comparison. For the photon beam energy fluence, Fig. 5 shows fluence spectra of the 6 MV flattened and unflattened beams at the water phantom surface. The variations of photon energy fluence spectra in the bone heterogeneity are shown in Fig. 6(a) for the flattened beams at the water and bone phantom surface. Similarly, Fig. 6(b) shows photon energy fluence spectra for the unflattened beams. Fig. 7(a) and (b) shows the photon energy fluence

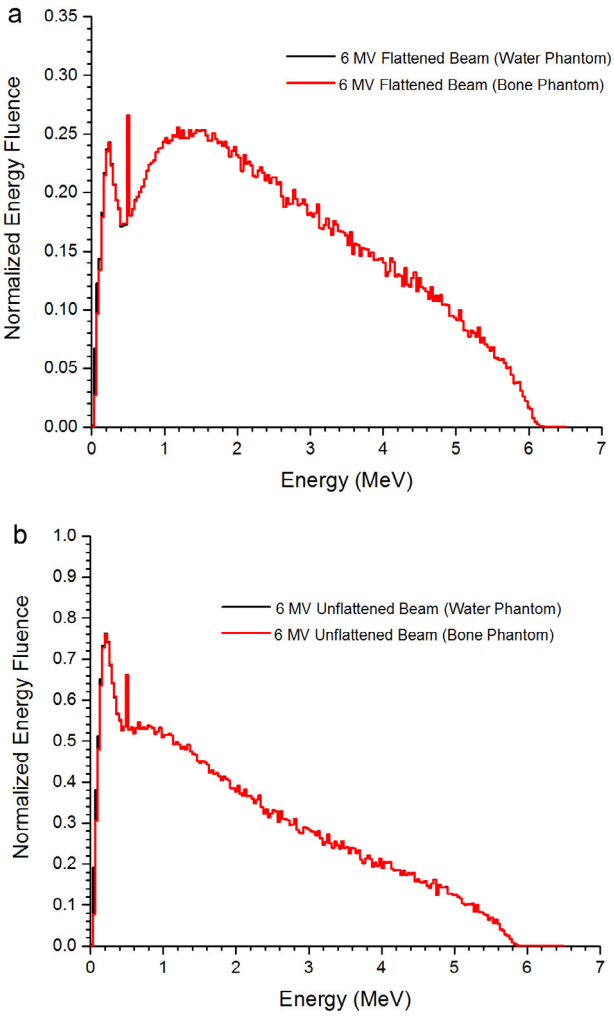

Fig. 6 – Photon energy fluence spectra at the water and bone phantom surface for the 6 MV (a) flattened and (b) unflattened photon beams.

spectra of the flattened and unflattened beams in different beam angles (0°, 15°, 30° and 45°) at the water phantom surface, while Fig. 7(c) and (d) shows the corresponding spectra with the same beam geometry using the bone phantom. All photon energy fluence in Figs. 5–7 was normalized to the maximum intensity in all beam calculation geometries. Variations of mean photon beam energy in beam angle for the flattened and unflattened beams at the water and bone phantom surface are shown in Fig. 8.

4.1. *Effect of the flattening filter on the surface photon energy and energy fluence spectra*

The effect of flattening filter on the photon beam energy spectra at the water phantom surface is shown in Fig. 2. The unflattened photon beam contained more number of photons, mostly concentrated in the low-energy range (0–2 MeV). When the flattening filter was used, those low-energy photons were absorbed resulting in a flattened beam spectral curve with lower intensity. For the photon energy fluence comparison, Fig. 5 shows that in the absence of flattening filter, more energy

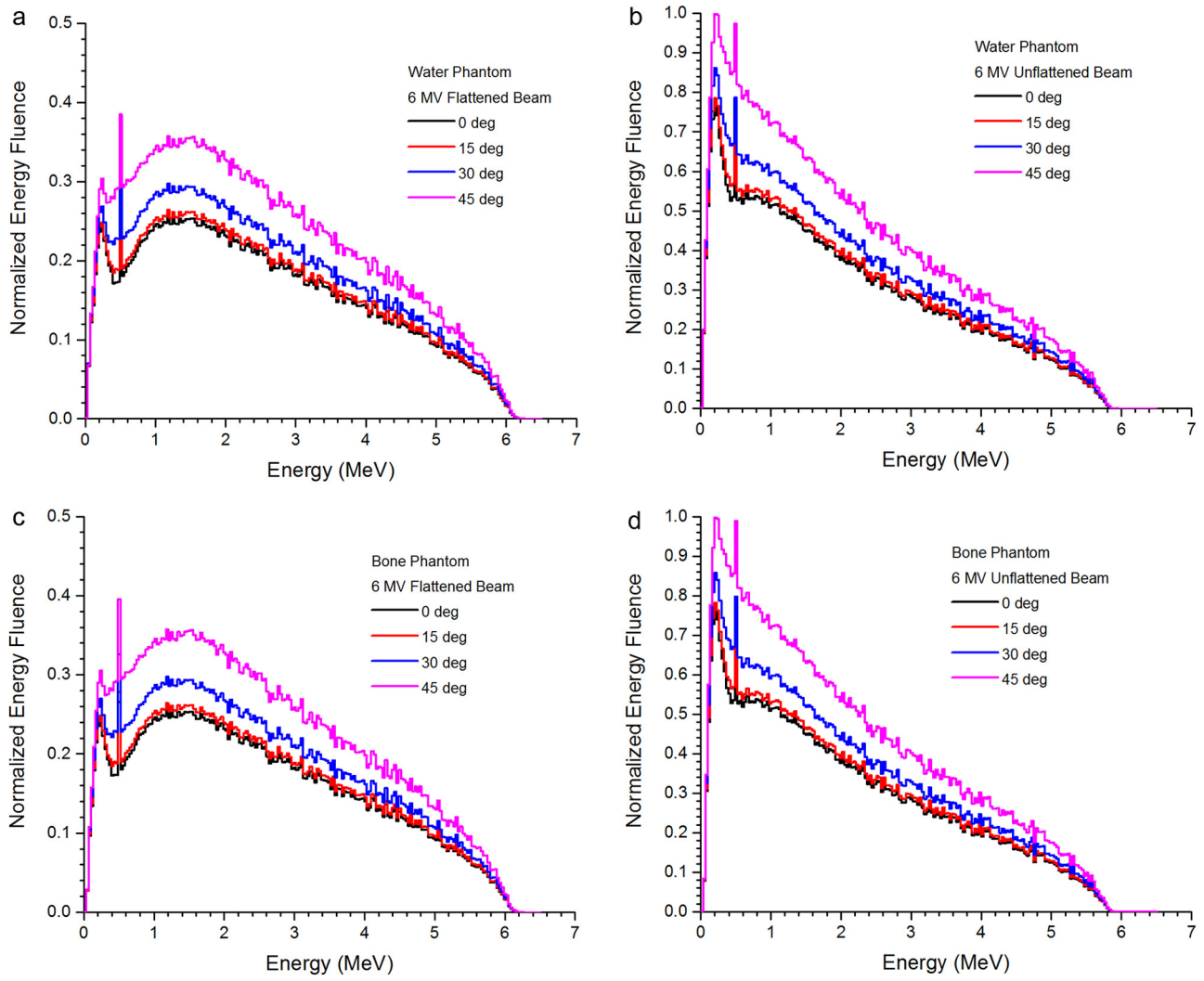

Fig. 7 – The variations of photon energy fluence spectra in beam angle for the 6 MV (a) flattened photon beams (water phantom), (b) unflattened photon beams (water phantom), (c) flattened photon beams (bone phantom) and (d) unflattened photon beams (bone phantom).

fluence was found in the low-energy range. As the increase of photon number was more significant in the low-energy range, and the energy fluence counted on the total energy contributed by photons, the increase of energy fluence was found decreased with an increase of photon beam energy. Moreover, the difference between the flattened and unflattened photon beams in Fig. 5 was less significant compared to that in Fig. 2. This is because even there were more low-energy photons found in Fig. 2 without using the flattening filter, the increase of energy fluence in Fig. 5 was less because the energy of each photon was low.

4.2. *Effect of the bone heterogeneity on the surface photon energy and energy fluence spectra*

In Fig. 3(a) and (b) showing the photon energy spectra of the flattened and unflattened beams at the water and bone phantom surface, it is seen that there was a small increase of photons in the water phantom. This shows that the presence of bone absorbed some low-energy photons from the beam leading to a decrease of bone backscatters. Since this effect occurred in both the flattened and unflattened photon beams, the presence of flattening filter did not affect the bone backscatters. However, considering the related photon energy fluence for the flattened and unflattened beams in Fig. 6(a), and (b), it can be seen the two spectral curves (water and bone phantom) were almost the same, even there was a small decrease of photons observed in the bone phantom (Fig. 3). This indicates that the bone heterogeneity, though slightly reduced the number of photons at the phantom surface, did not affect the energy fluence and hence the surface dose deposition.

4.3. *Effect of the beam obliquity on the surface photon energy and energy fluence spectra*

The variations of photon beam energy and energy fluence spectra in beam angle are shown in Fig. 4(a) and (b) for the flattened and unflattened beams in the water phantom. When the beam angle increased, more photons were found at the

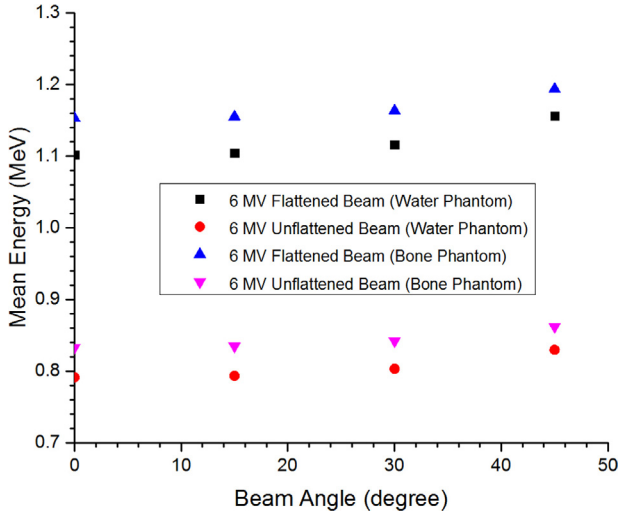

Fig. 8 – The variations of mean photon beam energy in beam angle at the water and bone phantom surface for the 6 MV flattened and unflattened photon beams.

phantom surface leading to surface dose enhancement. The increase of photon was also observed concentrated in the low-energy range. On the other hand, the extent of increased photons was found getting more as the beam angle increased. For both the flattened and unflattened photon beams, the energy spectra were very similar between beam angles equal to 0° and 15°. When the bone was added to the water phantom (Fig. 4(c) and (d)), the change of photon energy spectra was very small compared to without the bone. This shows that the bone heterogeneity was not sensitive to the beam obliquity regarding the photon beam energy spectra.

For variations of the surface photon energy fluence in the beam obliquity, it is seen in Fig. 7(a) and (b) that the energy fluence increased with beam angle for the flattened and unflattened beams in the water phantom. Similar to Fig. 4(a) and (b), it is found that the increase of energy fluence from beam angles of 0° to 15° was smaller compared to larger angles. This indicates that the variation of patient's external curvature (typically within the beam obliquity between 0° and 15°) would not affect the surface dose significantly. Moreover, the energy fluence was found increased more in the low-energy range than high-energy as beam angle increased. Comparing Fig. 7(a) and (b), it can be seen that the unflattened beam had more energy fluence in the low-energy range because of the absence of flattening filter. When the water phantom was changed to bone phantom with the same beam geometry in Fig. 7(c) and (d), the variation of energy fluence with and without the bone heterogeneity was small. This shows that the bone absorption of photons did not affect the energy fluence significantly. This may be because the increased number of low-energy photons could only result in very low energy fluence at the phantom surface. Similar to the water phantom, when the beam angle increased, the energy fluence was increased more and more in the bone phantom. The increase of energy fluence from beam angle of 0° to 15° was therefore less significant compared to from 30° to 45°.

For the mean energy of flattened and unflattened photon beams varying with the beam angle, it is found in Fig. 8 that the flattened photon beams had higher mean photon energies than the unflattened. This is because of the increase of beam hardening due to the presence of the flattening filter. In addition, all photon beam energies were seen to increase with an increase of the beam angle. This indicates that the photon beam became hardened when the beam angle increased. In the presence of bone heterogeneity, the mean photon beam energy increased in Fig. 8. This is because the bone absorbed some low-energy photons backscattered to the phantom surface. This resulted in a more hardened beam and an increase of mean photon beam energy. In Fig. 8, differences of the mean photon beam energies between the water and bone phantom for the flattened and unflattened beams were small. This shows that the presence of flattening filter did not affect the bone backscatters to the phantom surfaces.

5. Conclusions

Spectral photon energy and energy fluence studies were carried out on different beam obliquity using the flattened and unflattened beams at the water and bone phantom surface. It is found that the unflattened photon beam contained more photons and energy fluence compared to the flattened beam. The increase of photons was mainly concentrated in the low-energy range of 0–2 MeV. Comparing the water and bone phantom, more low-energy photons (<0.4 MeV) were found at the water phantom surface. This shows that the bone absorbed those photons from the beams (flattened and unflattened), though the heterogeneity did not affect the energy fluence at the surface. When the beam angle was increased, the number of photon and energy fluence increased at the phantom surface. The mean photon beam energy increased with an increase of beam angle, showing photon beam became more hardened in larger beam angle. The presence of bone also increased the mean photon beam energy, as the bone absorbed some low-energy photons backscattered to the phantom surface and resulted in a more hardened photon beam. The new calculated spectral data in this study should help to understand previously published results, in the radiation physics aspect, concerning variations of beam quality in the presence of bone heterogeneity, and beam obliquity using the flattened and unflattened photon beams.

Conflict of interest

None declared.

Financial disclosure

None declared.

Acknowledgements

The authors would like to acknowledge the Varian Monte Carlo research team for generating the phase-space data of the TrueBEAM linear accelerator available in this study.

REFERENCES

1. Cashmore J. The characterization of unflattened photon beams from a 6 MV linear accelerator. *Phys Med Biol* 2008;**53**:1933–46.
2. Cashmore J, Ramtohul M, Ford D. Lowering whole-body radiation doses in pediatric intensity-modulated radiotherapy through the use of unflattened photon beams. *Int J Radiat Oncol Biol Phys* 2011;**80**:1220–7.
3. Kragl G, Baier F, Lutz S, et al. Flattening filter free beams in SBRT and IMRT: dosimetric assessment of peripheral doses. *Z Med Phys* 2011;**21**:91–101.
4. Spruijt KH, Dahele M, Cuijpers JP, et al. Flattening filter free vs flattened beams for breast irradiation. *Int J Radiat Oncol Biol Phys* 2013;**85**:506–13.
5. Zwahlen DR, Lang S, Hrbacek J, et al. The use of photon beams of a flattening filter-free linear accelerator for hypofractionated volumetric modulated arc therapy in localized prostate cancer. *Int J Radiat Oncol Biol Phys* 2012;**83**:1655–60.
6. Fu WH, Dai JR, Hu YM, Han DS, Song YX. Delivery time comparison for intensity-modulated radiation therapy with/without flattening filter: a planning study. *Phys Med Biol* 2004;**49**:1535–47.
7. Parasai EI, Pearson D, Kvale T. Consequences of removing the flattening filter from linacs in generating high dose rate photon beams for clinical applications: a Monte Carlo study verified by measurement. *Nucl Instrum Methods Phys Res B* 2007;**261**:735–59.
8. Georg D, Knoos T, McClean B. Current status and future perspective of flattening filter free photon beams. *Med Phys* 2011;**38**:1280–93.
9. Stathakis S, Esquivel C, Gutierrez A, Buckey CR, Papanikolaou N. Treatment planning and delivery of IMRT using 6 and 18 MV photon beams without flattening filter. *Appl Radiat Isot* 2009;**67**:1629–37.
10. Navarria P, Ascolese AM, Mancosu P, et al. Volumetric modulated arc therapy with flattening filter free (FFF) beams for stereotactic body radiation therapy (SBRT) in patients with medically inoperable early stage non small cell lung cancer (NSCLC). *Radiother Oncol* 2013;**107**:414–8.
11. O'Brien PF, Gillies BA, Schwartz M, Young C, Davey P. Radiosurgery with unflattened 6 MV photon beams. *Med Phys* 1991;**18**:519–21.
12. Presendergast BM, Fiveash JB, Popple RA, et al. Flattening filter-free linac improves treatment delivery efficiency in stereotactic body radiation therapy. *J Appl Clin Med Phys* 2012;**14**:64–71.
13. Scorsetti M, Alongi F, Castiglioni S, et al. Feasibility and early clinical assessment of flattening filter free (FFF) based stereotactic body radiotherapy (SBRT) treatments. *Radiat Oncol* 2011;**6**:113.
14. Vassiliev ON, Kry SF, Chang JY, Balter PA, Titt U, Mohan R. Stereotactic radiotherapy for lung cancer using a flattening filter free Clinac. *J Appl Clin Med Phys* 2009;**10**:14–21.
15. Clerici FAE, Pentimalli S, Mancosu P, Scorsetti M. Initial experience of hypofractionated radiation retreatment with true beam and flattening filter free beam in selected case reports of recurrent nasopharyngeal carcinoma. *Rep Pract Oncol Radiother* 2012;**17**:262–8.
16. Mesbahi A, Nejad FS. Monte Carlo study on a flattening filter-free 18-MV photon beam of a medical linear accelerator. *Radiat Med* 2008;**26**:331–6.
17. Sixel KE, Faddegon BA. Calculation of X-ray spectra for radiosurgical beams. *Med Phys* 1995;**22**:1657–66.
18. Titt U, Vassiliev ON, Ponisch F, Dong L, Liu H, Mohan R. A flattening filter free photon treatment concept evaluation with Monte Carlo. *Med Phys* 2006;**33**:1595–602.
19. Wang Y, Khan MK, Ting JY, Easterling SB. Surface dose investigation of the flattening filter-free photon beams. *Int J Radiat Oncol Biol Phys* 2011;**83**:281–5.
20. Chow JCL, Owrangi AM. Dosimetric dependences of bone heterogeneity and beam angle on the unflattened and flattened photon beams: a Monte Carlo comparison. *Radiat Phys Chem* 2014;**101**:46–52.
21. Chow JCL, Grigorov GN. Surface dosimetry for oblique tangential photon beams: a Monte Carlo simulation study. *Med Phys* 2007;**35**:70–6.
22. Chow JCL, Owrangi AM. Monte Carlo study on mucosal dose in oral and nasal cavity using photon beams with small field. *J Radiother Pract* 2011;**10**:261–71.
23. Chow JCL, Owrangi AM. Dependences of mucosal dose on photon beams in head-and-neck intensity-modulated radiation therapy: a Monte Carlo study. *Med Dosim* 2012;**37**:195–200.
24. Chow JCL, Jiang R, Leung MKK. Dosimetry of oblique tangential photon beams calculated by superposition/convolution algorithms: a Monte Carlo evaluation. *J Appl Clin Med Phys* 2010;**12**:108–21.
25. Dalaryd M, Kragl G, Ceberg C, et al. A Monte Carlo study of a flattening filter-free linear accelerator verified with measurements. *Phys Med Biol* 2010;**55**:7333–44.
26. Ponisch F, Titt U, Vassiliev ON, Kry SF, Mohan R. Properties of unflattened photon beams shaped by a multileaf collimator. *Med Phys* 2006;**33**:1738–46.
27. Vassiliev ON, Titt U, Kry SF, Ponish F. Monte Carlo study of photon fields from a flattening filter-free clinical accelerator. *Med Phys* 2006;**33**:820–7.
28. ICRP report 23 *ICRP report on the task group on reference man: anatomical, physiological and metabolic characteristics*. New York: ICRP; 1975.
29. Agostinelli S, Allison J, Amako K, et al. GEANT4 – a simulation toolkit. *Nucl Instrum Methods Phys Res A* 2003;**506**:250–303.
30. KawrakowF I., Rogers DWO, technical report PIRS-701 *The EGSnrc code system: Monte Carlo simulation of electron and photon transport*. Ottawa, Canada: National Research Council of Canada; 2000.
31. Constantin M, Sawkey D, Mansfield S, Salop A. Extended True-Beam patient-independent phase space library for the 6x, 6xFFF, 10x, and 10xFFF radiotherapy beams calculations. *Med Phys* 2011;**38**:3642.
32. Constantin M, Perl J, LoSasso T, et al. Modeling the TrueBeam linac using CAD to Geant4 geometry implementation: dose and IAEA-compliant phase space calculations. *Med Phys* 2011;**38**:4018–24.
33. Sardari D, Samavat H, Esmaeeli A, Maleki R. Measurement of depth-dose of linear accelerator and simulation by use of GEANT4 computer code. *Rep Pract Oncol Radiother* 2010;**15**:64–8.
34. Constantin M. http://my.varian.com/montecarlo_reg/2; 2011.
35. Rogers DWO, Walters BRB, Ding GX, Sheikh-Bagheri D, Zhang G, NRCC report No. PIRS-0509(a)Rev L *BEAMnrc user manual*. Ottawa: National Research Council of Canada; 2011.
36. Chow JCL, Owrangi AM. Effect of the bone heterogeneity on the unflattened and flattened photon beam dosimetry: a Monte Carlo comparison. *Med Phys* 2014;**41**:255.